Paper # 139LF-0021 **Topic: Laminar Flames**

Western States Section of the Combustion Institute - Spring 2016 Meeting
Hosted by University of Washington
March 21-22, 2016.

Effects of updated transport properties of singlet oxygen species on steady laminar flame simulations

Daniel I. Pineda[1] *Jyh-Yuan Chen*[1]

[1]*Department of Mechanical Engineering, University of California, Berkeley, United States*

A current problem is distinguishing the relative contributions of chemical kinetic and transport effects to the enhancement of plasma-assisted combustion. As numerical investigations in plasma-assisted combustion move to simulations in one or more dimensions, the transport properties of excited-state species thought to contribute to the combustion enhancement will need to be determined to accurately model these systems and discern their chemical kinetic contribution to the enhancement. We provide estimates of the intermolecular interaction energies of singlet oxygen ($O_2(a^1\Delta_g)$ and $O_2(b^1\Sigma_g^+)$) using ab initio quantum chemistry methods, and find that the transport properties derived from these interaction energies are substantially different from those of the corresponding ground state. One-dimensional simulations of both premixed and non-premixed steady low-pressure methane flames seeded with 2.5% $O_2(a^1\Delta_g)$ in the oxidizer were performed. Results indicate that updating the transport properties of the singlet oxygen species has a very small effect on flame speed and structure, but that this effect is largest in premixed flame simulations due to reactions of $O_2(a^1\Delta_g)$ with H atoms.

1 Introduction

It has been known for some time that combustion can be influenced by electric fields [1]. Plasma-Assisted Combustion (PAC)—the generation or enhancement of plasma in a combustion environment through the use of microwaves, radio frequency waves, dielectric barrier discharges, nanosecond pulse discharges, and other electric discharges—has been shown to reduce ignition delay times and increase flame speeds under various conditions and is an active area of research [2, 3, 4]. While it is clear that applying electric fields to ignitable mixtures and flames can enhance combustion, the relative contributions to combustion enhancement from both chemical kinetics and transport processes remains uncertain, particularly in systems that utilize these techniques in macroscale combustion applications [5, 6]. These effects in experimental investigations of PAC are typically highly coupled, making it difficult to discern the underlying physics, though some components of enhancement in isolation are beginning to be understood.

Excited state species created in non-thermal plasmas via electron impact excitation reactions participate in combustion reactions and are generally more reactive [7, 8]. A particular electronically-excited species, singlet oxygen ($O_2(a^1\Delta_g)$), has been experimentally confirmed to enhance flame propagation [9, 10]. Kinetic models considering reactions with $O_2(a^1\Delta_g)$ have also predicted increases in flame speed [9, 11, 12, 10, 13], though many have been shown to overestimate the purported flame speed enhancement [9, 10, 13]. While one of the emerging reasons for this overestimation seems to be a lack of consideration of quenching reactions [9, 10, 14], more research is necessary to explain the experimentally observed enhancement.

In many kinetic studies considering spatial dimensions, researchers have assumed that the transport properties of excited state species are the same as those of their ground state counterparts [12, 8], though some have accounted for changes in molecule size [11]. While recent progress has been made in accounting for the transport properties of ions in PAC [15], there is a scarcity of information available in the literature regarding the interaction energies of these electronically-excited state molecules, and they have even been requested by other researchers [12]. Early in the history of ab initio quantum chemistry calculations, Buckingham and Dalgarno [16] showed that the interaction of ground state helium atoms and the interactions of helium with metastable triplet helium are significantly different, with a difference in well depths on the order of 1000. As such, there is reason to suspect that the interaction energies of $O_2(a^1\Delta_g)$ and $O_2(b^1\Sigma_g^+)$ are significantly different from the corresponding ground state, $O_2(X^3\Sigma_g^-)$, and that this difference will result in appreciably different transport properties.

As researchers continue to study the chemical kinetic behavior of plasma-assisted flames with excited species with increasing accuracy, they will need updated transport properties to inform the calculations of rate constants based on their experiments. In this work, we use ab initio quantum chemistry methods to determine the interaction energies and corresponding transport parameters of these species, and apply these updated parameters to steady one-dimensional flame simulations to determine their effect on the flame speed and structure. For this study, the interactions of the two lowest lying excited singlet states of oxygen, $O_2(a^1\Delta_g)$ and $O_2(b^1\Sigma_g^+)$, are presented. Our goal is to revive a discussion in the community regarding these excited-state molecular interactions in a combustion context.

2 Method

The long range interactions of molecules are predominantly the result of dispersion interactions between the electrons of different molecules as the molecules near one another [17]. These interaction energies and the resulting transport properties can be obtained from experiments on pure substances that determine the second coefficient in the virial equation of state [18, 17]. However, such experiments are difficult to conduct for excited molecules and so methods such as molecular beam scattering [19] have been used, but still present additional detection challenges. The goal of these experiments for the purposes relevant to combustion modeling is to determine the interaction energies and extract the collision diameter σ and interaction potential well depth ϵ utilized (for nonpolar molecules) in the 6-12 Lennard-Jones expression for intermolecular potential energy

$$V(r) = -4\epsilon\left[\left(\frac{\sigma}{r}\right)^{12} - \left(\frac{\sigma}{r}\right)^{6}\right] \tag{1}$$

where r is the intermolecular distance between the interacting molecules. For non-polar molecules, the diffusivity, thermal conductivity, and viscosity are dependent only on temperature, pressure, molecular mass, and the values of σ and ϵ. When interactions with polar molecules are considered, the dipole moment μ and the polarizability of the molecule α are relevant [18]. These properties can be calculated via quantum mechanical methods described in Section 2.1. None of the molecules considered here are polar, and so μ is assumed to be 0 for all the quantum mechanical calculations presented. The interactions of the molecules in a pure substance can be applied to mixtures through combining rules with reasonable accuracy [20].

2.1 Ab initio calculations

To determine the interaction energies for excited-state species of interest, we performed ab initio quantum chemistry calculations for the species using GAMESS [21]. Similar calculations have been performed by other researchers seeking to obtain Lennard-Jones parameters for combustion applications with modest success, obtaining parameters within 10% of experimental values [22]. We seek a solution of the time-independent Schödinger Equation for a multielectron system with electron positions given by $\vec{r}_i$ moving about a system of nuclei with positions specified by $\vec{R}_j$ [23]:

$$H\mathbf{\Psi}(\vec{r}_i, \vec{R}_j) = E\mathbf{\Psi}(\vec{r}, \vec{R}_j) \tag{2}$$

All calculations presented here apply the Born-Oppenheimer approximation, which posits that the motions of electrons are so much faster than the motions of the nuclei relative to one another that for most systems, the total wavefunction $\mathbf{\Psi}(\vec{r}_i, \vec{R})$ can be separated into electronic and nuclear wavefunctions:

$$\mathbf{\Psi}(\vec{r}_i, \vec{R}_j) = \Psi(\vec{r}_i; \vec{R}_j)\chi(\vec{R}_j) \tag{3}$$

The calculations performed approximate a solution for $\Psi(\vec{r}_i; \vec{R}_j)$, fixing the positions of the nuclei and calculating the resulting energies. Solving the wavefunction for several different values of $\vec{R}_j$ results in the potential energy surface of a molecular collision.

To capture the weak intermolecular dispersion forces, the augmented correlation-consistent polarized quadruple-zeta valence (aug-cc-pVQZ) basis sets [24] were used for all calculations, performed at the Restricted Open-Shell Hartree-Fock (ROHF) level of theory [25] with electron configuration interaction (CI) calculated using the Graphical Unitary Group Approach (GUGA) [26]. In this method, the spin multiplicity of the system is both specified and inferred from the individual molecular orbitals (MOs), which can be doubly occupied, singly occupied (with an alpha or beta electron spin), or empty.

2.1.1 Polarizabilities

For each diatomic molecule, we determined the equilibrium geometry by minimizing the total energy as a function of distance between the two atoms. Once this equilibrium bond length was determined, we performed finite-field polarizability calculations [27] to obtain the polarizabilities of the molecules. For the diatomic O_2 and nitrogen (N_2), the Fully-Optimized Reaction Space (FORS) of 10 MOs was considered, and the properties of $O_2(b^1\Sigma_g^+)$ were obtained by evaluating the first excited state of $O_2(a^1\Delta_g)$. For the monatomic species Helium (He) and Neon (Ne), the FORS of 2 and 6 MOs, respectively, were considered.

2.1.2 Molecular interactions

For each collision calculation, two molecules of a specified electronic state were prescribed in a relative orientation and incrementally moved closer to one another; the resulting energy was determined at each intermolecular distance to obtain a potential energy curve—the interaction energy. Calculations report the total absolute energy, so the interaction energy was determined by

subtracting the potential energy curve from two times the energy of a single molecule, E_{single}, representing a condition where the two molecules are far enough apart to be completely independent of one another:

$$V(r) = E(r) - 2E_{single} \tag{4}$$

For the noble gases He and Ne, the FORS of all MOs occupied by electrons were considered ($1s^2$ and $1s^2 2s^2 2p^6$, respectively) with two additional valence orbitals beyond the highest occupied orbital in the reference state on each atom to capture the dispersion interaction. For the diatomic O_2 and N_2, *half* of the FORS of 16 MOs was employed (8 for each molecule). The 1σ MOs of each diatomic molecule were assumed to not contribute significantly to the long-range intermolecular interactions. For two O_2 molecules, no significant difference was observed for a FORS (24 electrons in 16 MOs) versus using half of a FORS, and the FORS for 16 MOs in N_2 (20 electrons in 16 MOs) is currently not computationally feasible utilizing the GUGA method. The interaction of two $O_2(b^1\Sigma_g^+)$ molecules was obtained by evaluating the second (doubly) excited state of two $O_2(a^1\Delta_g)$ molecules.

For a given collision orientation, ϵ is determined by finding the value of r_{min} that minimizes Equation 4 and assigning

$$\epsilon = V(r_{min}) \tag{5}$$

Likewise, σ is determined as the intermolecular distance (smaller than the distance of minimum energy) for which Equation 4 changes sign from negative to positive:

$$V(\sigma < r_{min}) = 0 \tag{6}$$

For the diatomic molecules, only head-on collisions along a Cartesian axis aligned either parallel or perpendicular to the molecular bond of each molecule were considered, and the bond lengths of each of the molecules were assumed to not change throughout the collision. Similar to the one-dimensional minimization technique utilized by [22], the resulting values of ϵ and σ from each type of collision are weighted accordingly, to produce "average" values of ϵ and σ that would be observed experimentally. The determination of the weighting is discussed in the Appendix. While a significant simplification (two molecules can collide in an infinite number of orientations), such a method still allows for direct comparison of interaction energies between molecules in different electronic states.

2.2 One dimensional steady flame calculations

The CHEMKIN-II [28] applications PREMIX [29] and OPPDIF [30] were used to compute steady one-dimensional low pressure flames seeded with $O_2(a^1\Delta_g)$ in the oxidizer. For all simulations, the oxidizer was 79% Argon (Ar), 18.5% O_2, and 2.5% $O_2(a^1\Delta_g)$. This mole fraction of $O_2(a^1\Delta_g)$ was chosen because it is representative of the upper limit of what has been considered in other numerical studies [12, 8, 11], and the conditions were chosen to be representative of conditions under which kinetic experiments in PAC are often performed. A CH_4-air mechanism used by DeFilippo [31] based on GRI-Mech 3.0 [32] containing reactions with excited species was used for all computations, and the simulations were performed with multicomponent transport. For both the premixed and non-premixed simulations, two sets of calculations are presented—one assuming

that $O_2(a^1\Delta_g)$ and $O_2(b^1\Sigma_g^+)$ possess the same values of σ, ϵ/k_B, and α as $O_2(X^3\Sigma_g^-)$, and another with values corresponding to the results of the quantum chemistry calculations. The rotational relaxation constants Z_{rot} and thermodynamic properties for $O_2(a^1\Delta_g)$ and $O_2(b^1\Sigma_g^+)$ were assumed to be the same as those of $O_2(X^3\Sigma_g^-)$, however. No other variables are altered in the mechanism.

2.2.1 Premixed flame simulations

For the premixed flame simulations utilizing PREMIX, the pressure was 3 kPa and the inlet temperature was 300 K. The flame speed was calculated for equivalence ratios ranging from $\phi = 0.65$ to $\phi = 1.35$, and the structure of the mole fractions and rates of production as a function of distance were calculated as well.

2.2.2 Non-premixed flame simulations

For the non-premixed flame simulations utilizing OPPDIF, the pressure was 5 kPa and the temperature of the fuel inlet was 300 K, while the temperature of the oxidizer inlet was 600 K. Steady flame solutions were not obtained for pressures lower than 5 kPa. The length of the domain was 3 cm. The fuel inlet velocity was 20 cm/s and the oxidizer inlet velocity was 50 cm/s, resulting in a total strain rate of 23 s^{-1}. In addition to the mole fraction and rates of production as a function of distance, the rate of heat release is also calculated.

3 Results

3.1 Ab initio calculations

The results of the ab initio intermolecular interaction and polarizability calculations for different molecules are summarized in Table 1. Several ground state property calculations are presented and compared with published experimental data to demonstrate the confidence in the methods utilized.

Molecule	R_e [Å]	ϵ/k_B [K]	σ [Å]	α [Å^3]
He	N/A	11.54	2.874	0.197
Ne	N/A	31.79	2.966	0.417
$N_2(X^1\Sigma_g^+)$	1.070	89.17	4.115	1.769
$O_2(X^3\Sigma_g^-)$	1.175	100.5	3.695	1.493
$O_2(a^1\Delta_g)$	1.195	1836	2.769	1.434
$O_2(b^1\Sigma_g^+)$	1.235	1036	2.994	1.662

Table 1: Summary of transport properties determined by ab initio calculations

3.1.1 Ground state molecular interactions: He, Ne, $O_2(X^3\Sigma_g^-)$, and $N_2(X^1\Sigma_g^+)$

To gain confidence in the method discussed, the intermolecular potentials of ground state oxygen and nitrogen were calculated and compared with experimental data from the literature. The calculated bond lengths (R_e) for all diatomic molecules were within 3% of experimental values [17], and the bond lengths for O_2 follow the observed trend of becoming larger as the electronic energy increases. For He, the calculated potential well depth and collision diameter were within 13% and 12% of experimental values [17, 33], respectively. The calculated polarizability was within 7% of experimental values [17]. For Ne, the potential well depth, collision diameter, and polarizability were within 11%, 8%, and 8% of experimental values [17], respectively. For $O_2(X^3\Sigma_g^-)$, the calculated potential well depth, collision diameter, and polarizability were all within 7% of currently accepted values [33]. The calculated well depth, collision diameter, and polarizability for N_2 were within 9%, 14%, and 1%, respectively, of experimental values [33]. Based on these comparisons, we conservatively estimate an uncertainty in this method of 20%. Other researchers utilizing ab initio methods have also obtained values of σ that are generally larger than experimental values when using similar collision weighting techniques [22], so this was considered normal, especially considering the limited collision orientations used in this investigation.

3.1.2 Interaction of helium and metastable triplet helium

To gain confidence in applying the ab-inito method to the interaction of excited state molecules, we attempted to reproduce the conclusions of Buckingham and Dalgarno [16]. For these simulations, two He atoms were specified, and the interaction energies for the ground singlet state atom with a metastable triplet state atom were calculated for various internuclear distances. Shown in Figure

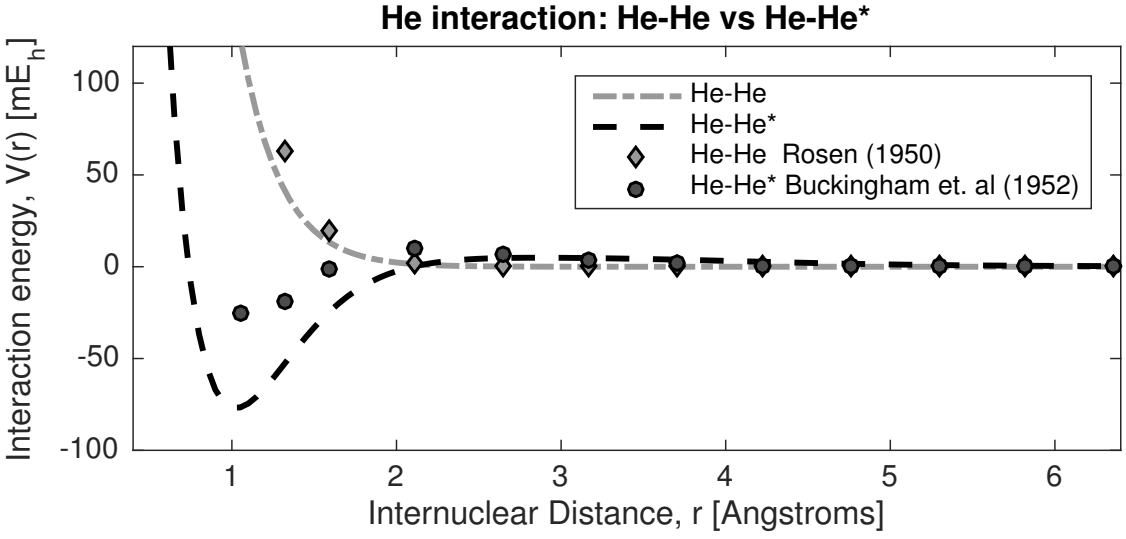

Figure 1: Interaction energies (units of milliHartree) as a function of internuclear distance for He atoms. Present calculations are shown as lines, while the calculations of Buckingham and Dalgarno [16] and Rosen [34] are shown with circles and diamonds, respectively.

1, the interaction energies for the He-He and the He-He* collisions are vastly different, confirming the conclusions of Buckingham and Dalgarno [16]. The interaction energies for two ground state He atoms were in good agreement with literature values, and the interaction energies for a ground state He atom with a metastable triplet He atom are in qualitative agreement, though the interaction energies calculated in this work are larger than those reported by Buckingham and Dalgarno [16]. This is likely due to the fact that the basis sets utilized in the present work are much greater in number and more diffuse. Additionally, the present work specified more orbitals in the CI calculation. Most importantly, the ab initio method captures the large differences in these interactions, and also captures the local maximum in the interaction curve that was also predicted by Buckingham and Dalgarno [16].

3.1.3 Interaction of excited singlet oxygen, $O_2(a^1\Delta_g)$ and $O_2(b^1\Sigma_g^+)$

With some confidence in the method based on the previous results, the interaction energies of two $O_2(a^1\Delta_g)$ molecules were calculated for the same collision orientations as the ground state diatomic molecules, and this was repeated for two $O_2(b^1\Sigma_g^+)$ molecules. The resulting 6-12 potential calculated from the collision weighting is shown in Figure 2 compared with the ground state potential, and the corresponding transport parameters are listed in Table 1. As with the interaction of

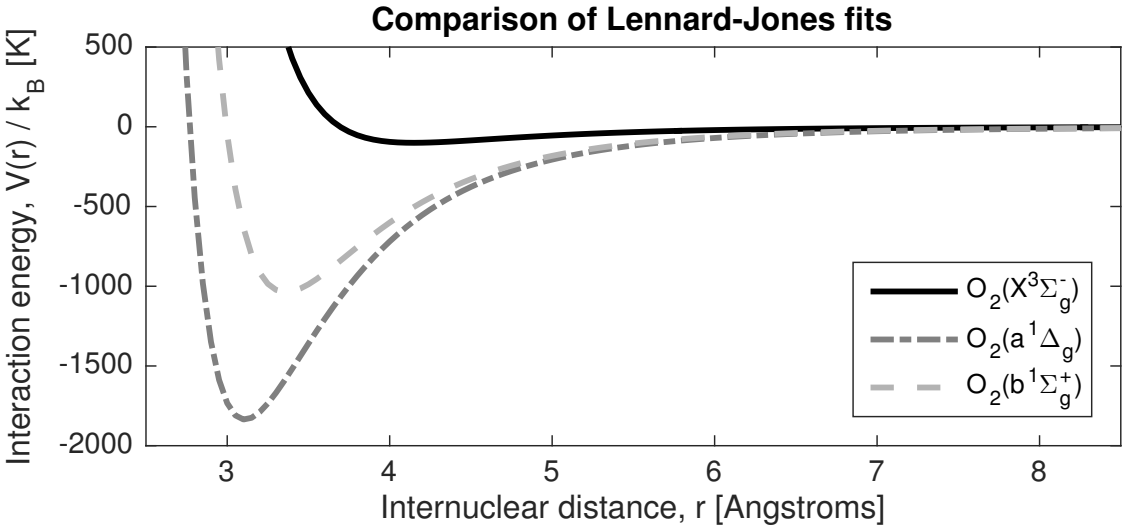

Figure 2: 6-12 Lennard-Jones fits of the calculated interaction energies for $O_2(X^3\Sigma_g^-)$, $O_2(a^1\Delta_g)$, and $O_2(b^1\Sigma_g^+)$

ground state He with metastable triplet He, the interactions are significantly larger than those of the ground state; this difference in well depth is a factor of about 18 for $O_2(a^1\Delta_g)$ and a factor of about 10 for $O_2(b^1\Sigma_g^+)$. The calculated collision diameters for the singlet oxygen species, however, are smaller than that of the ground state—approximately 24% smaller for $O_2(a^1\Delta_g)$ and 13% smaller for $O_2(b^1\Sigma_g^+)$.

3.2 One-dimensional flame calculation results

3.2.1 Premixed flames

The flame speeds calculated for the simulations with the 79% Ar-18.5% O_2-2.5% $O_2(a^1\Delta_g)$ oxidizer composition were approximately 27% larger than the simulations with 79% Ar-21% O_2 oxidizer composition near $\phi = 1$ and this increased to 34% near $\phi = 0.65$, confirming trends observed in other numerical kinetic investigations. Reasons for this enhancement have already been discussed in those studies [10, 13] and will not be further elaborated on here. Updating the transport properties to reflect the ab initio results resulted in a slight increase in the observed flame speed, shown in Figure 3.

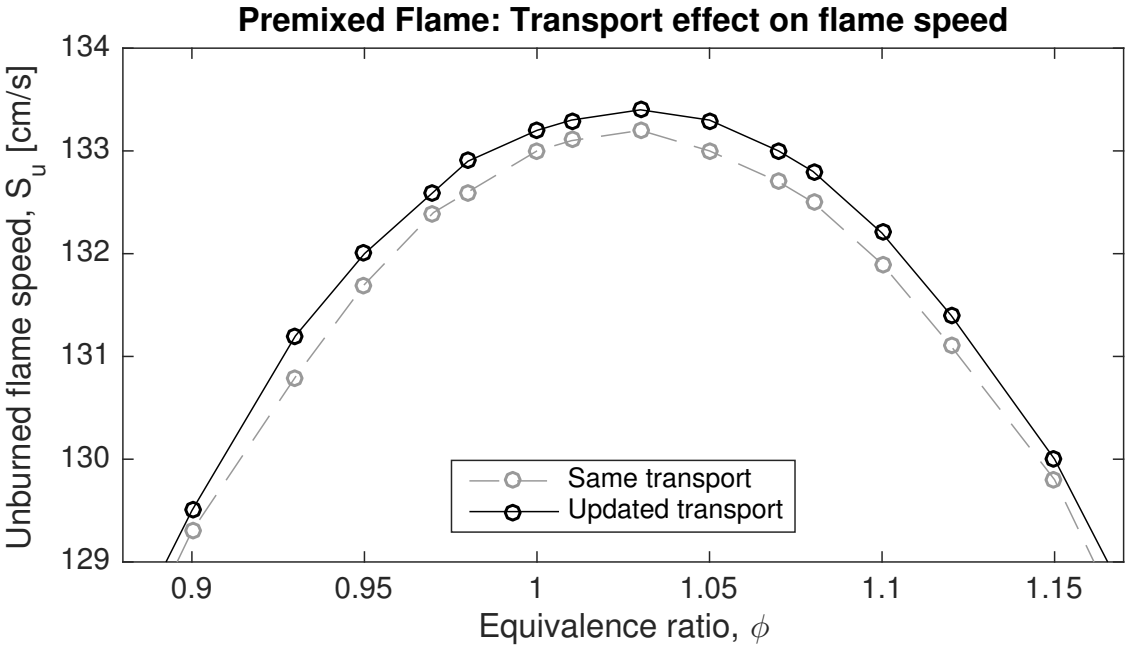

Figure 3: Effect of updated transport properties on the flame speed of a methane-oxygen-argon mixture as a function of equivalence ratio, 3 kPa. Solid lines correspond to updated transport properties of the singlet O_2 species, while the dashed lines correspond to a simulation in which the transport properties are assumed to be those of $O_2(X^3\Sigma_g^-)$.

On average, the resulting change in observed flame speed for these conditions was about 0.25%, though the effect was largest in leaner conditions. The transport effect on the structure of the flame is shown for mole fractions in Figure 4 and rates of production for $O_2(a^1\Delta_g)$ in Figure 5. In these plots, the x-axis is shifted so that the peak mole fraction of CH for each flame corresponds with $x = 0$ mm, since the electronic excitation of this molecule is associated with the typical blue color of CH_4 flames. The overall effect on the mole fractions shown in Figure 4 is small, with the most noticeable differences occurring for $O_2(a^1\Delta_g)$ and O. The mole fraction of $O_2(a^1\Delta_g)$ is increased by about 3% in the preheat region ($T \approx 500$ K) of the flame, before decreasing by approximately 6% about 5 mm later in the reaction zone ($T \approx 1700$ K). This suggests that the updated transport properties increase the "induction time" of $O_2(a^1\Delta_g)$ while also increasing

its rate of reaction after the delay. The mole fraction of O and OH in the preheat zone of the

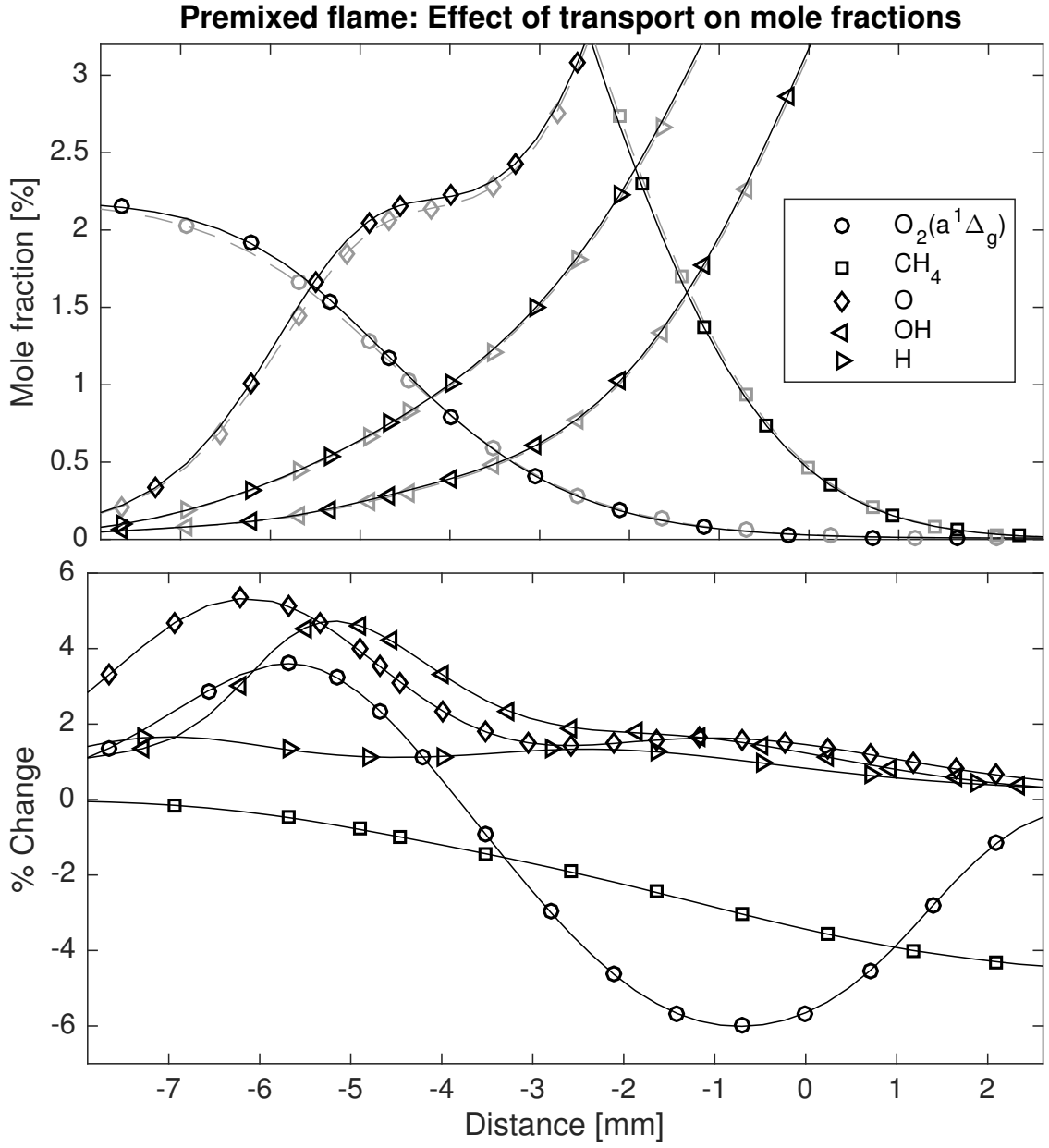

Figure 4: Effect of updated transport properties on mole fractions of $O_2(a^1\Delta_g)$, CH_4, O ($\times 40$), OH ($\times 5$), and H ($\times 5$). Solid lines correspond to updated transport properties of the singlet O_2 species, while the dashed lines correspond to a simulation in which the transport properties are assumed to be those of $O_2(X^3\Sigma_g^-)$.

flame are increased by approximately 5% and 4%, respectively, while the corresponding effect on H was smaller with an approximate 1% increase. In the reaction zone of the flame, the mole fraction of CH_4 is decreased by approximately 4%, indicating an increased consumption of the fuel. An examination of the rate of production for $O_2(a^1\Delta_g)$ shown in Figure 5 reveals that the

updated transport properties shift the peak of net consumption slightly (≈ 0.25 mm) earlier in the fresh gas, and that this is due almost entirely to a corresponding shift in the profile of the reaction $H + O_2(a^1\Delta_g) \rightleftharpoons OH + O$. Reactions such as the reverse reaction of $H_2O + O_2(a^1\Delta_g) \rightleftharpoons OH + HO_2$, which generates $O_2(a^1\Delta_g)$, are relatively unaffected by the updated transport properties, which is to be expected since for these reactions $O_2(a^1\Delta_g)$ is not a collision partner. Additionally, the peak net consumption rate of $O_2(a^1\Delta_g)$ increases by about 2%.

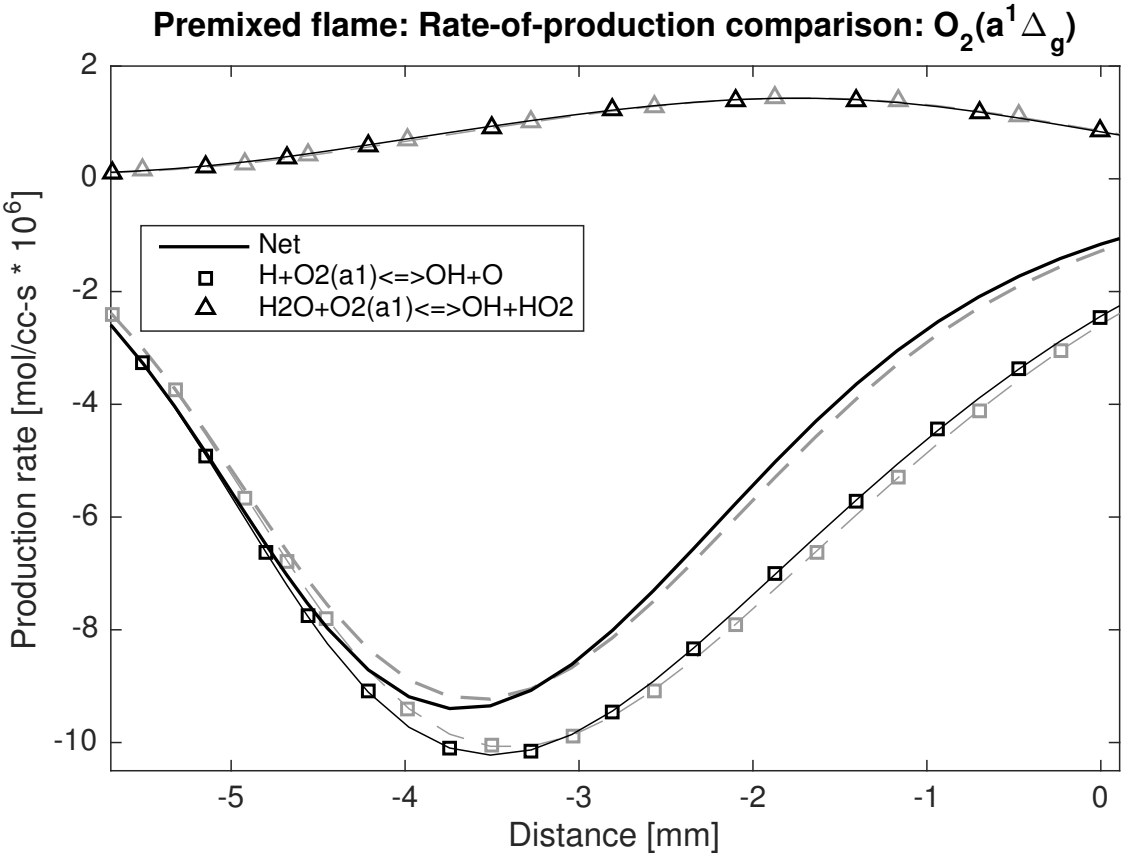

Figure 5: Effect of updated transport properties on rate of consumption of $O_2(a^1\Delta_g)$ as a function of distance for selected significant reactions. Solid lines correspond to updated transport properties of the singlet O_2 species, while the dashed lines correspond to a simulation in which the transport properties are assumed to be those of $O_2(X^3\Sigma_g^-)$.

3.2.2 Non-premixed flames

The results of the non-premixed flame simulation are shown in Figure 6, with the fuel entering from the left and the oxidizer entering from the right. Updating the transport properties is seen to have very little effect outside of the region closest to the oxidizer inlet. The mole fraction of $O_2(a^1\Delta_g)$, present in the inlet, rapidly decays, and the production rates of both $O_2(a^1\Delta_g)$ and $O_2(X^3\Sigma_g^-)$ reveal that the excited singlet oxygen species is converted to the ground state predominantly through collisional quenching. Small fractions of H present near the oxidizer inlet react with the $O_2(a^1\Delta_g)$

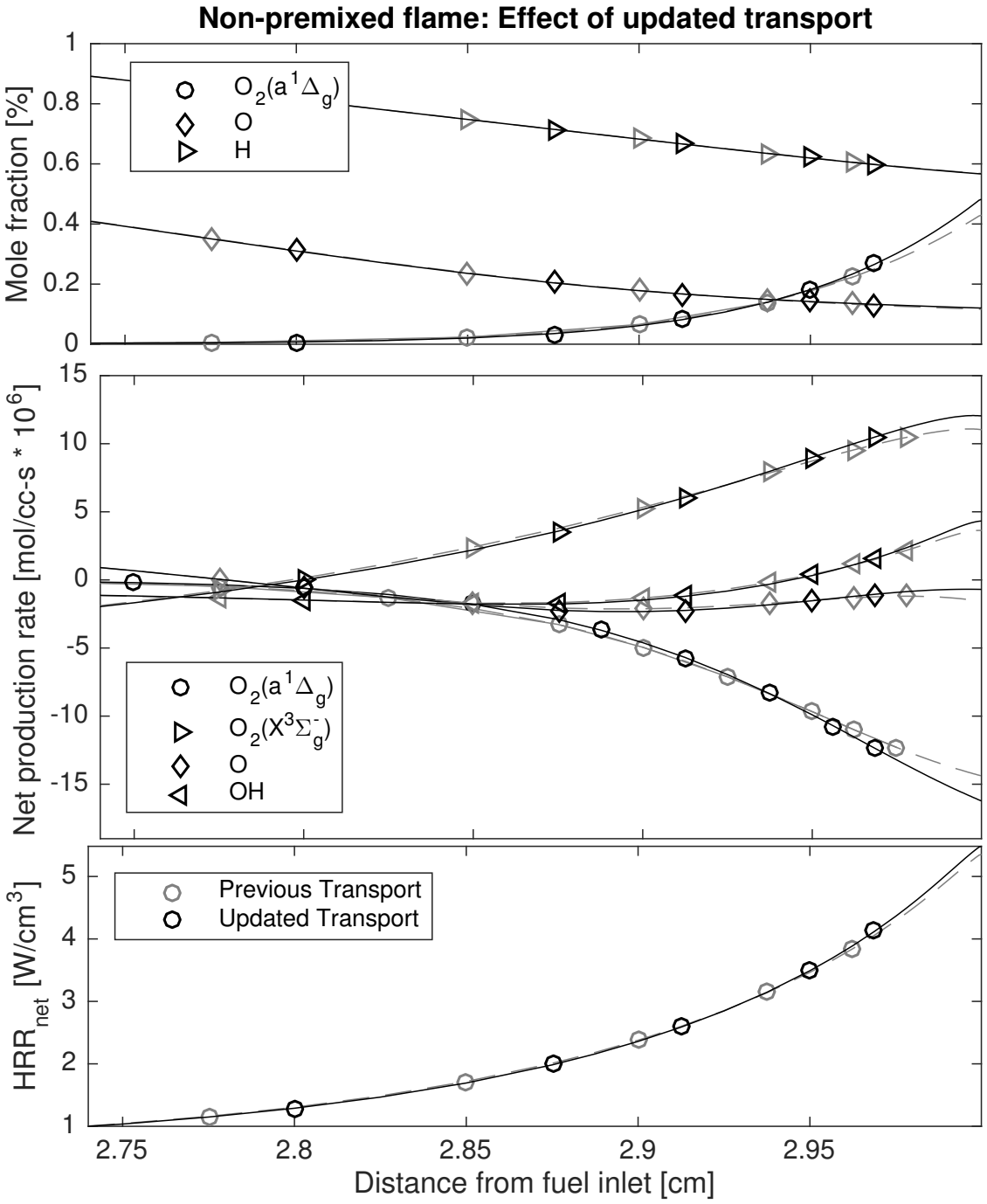

Figure 6: **Effect of updated transport properties on non-premixed flame near the oxidizer inlet. Top: mole fractions of selected species. Middle: rates of production for selected species. Bottom: net heat release rate. Solid lines correspond to updated transport properties of the singlet O_2 species, while the dashed lines correspond to a simulation in which the transport properties are assumed to be those of $O_2(X^3\Sigma_g^-)$.**

to form O and OH, but the rates of production are quite small and are not significantly affected by the updated transport. The positive net heat release rate near the oxidizer inlet is a product of the collisional quenching, since the excited state oxygen releases some energy in the form of translational energy upon de-excitation to the ground state. This rate of heat release is also not significantly impacted by updating the transport properties of the singlet oxygen species.

4 Discussion

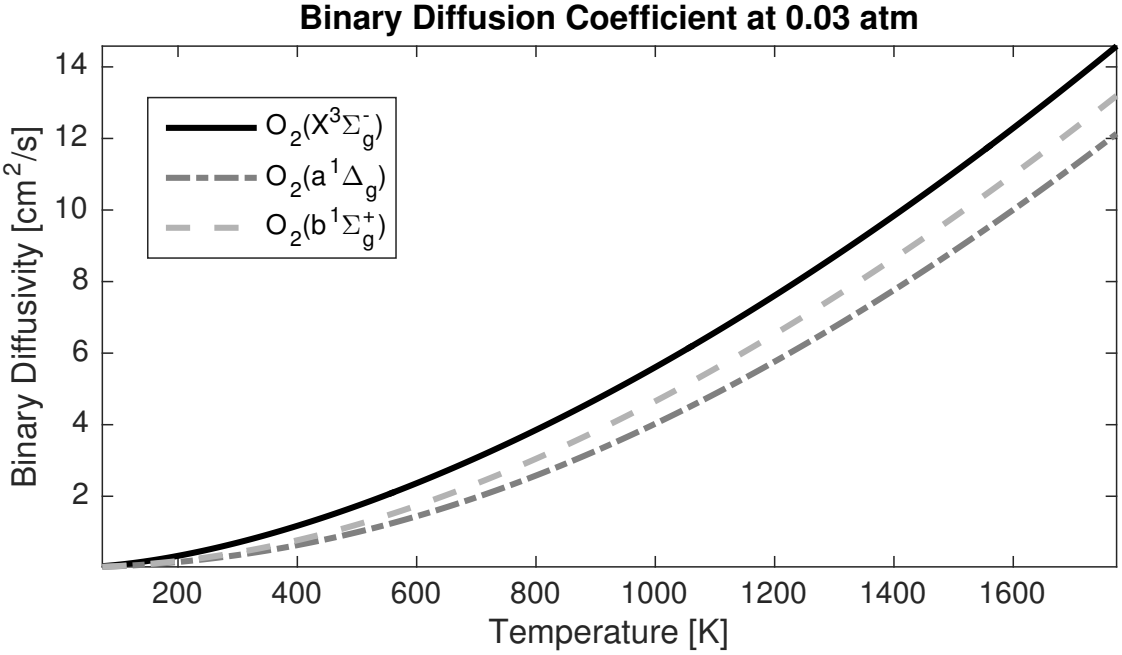

Figure 7: **Effect of updated transport properties on the binary diffusion coefficient of the oxygen species with methane at 0.03 atm for a range of temperature values.**

Shown in Figure 7, kinetic theory calculations based on the transport parameters listed in Table 1 result in binary diffusion coefficients (with CH_4) for $O_2(a^1\Delta_g)$ and $O_2(b^1\Sigma_g^+)$ that are roughly half and two-thirds, respectively, of the corresponding coefficient for the ground state at low to intermediate temperatures, though the magnitude of this difference is lower at larger temperatures. This explains the larger differences observed in the preheating zone of the premixed flame simulations, which had the cascading effect of increasing the local mole fraction of radical species and ultimately increasing the overall fuel consumption rates. Though the excited singlet oxygen species are not likely to directly interact with one another in the conditions discussed, the results of the He-He* interaction demonstrate that this large interaction occurs even when an excited molecule nears a ground state molecule, and this should be taken into consideration when evaluating the transport properties of gases that include excited species. Though both $O_2(a^1\Delta_g)$ and $O_2(b^1\Sigma_g^+)$ have smaller collision diameters than $O_2(X^3\Sigma_g^-)$, this does not increase the mobility of these species because the large well depth generated by the interaction of the electrons of the molecules traps them near one another. The reduced mobility of $O_2(a^1\Delta_g)$ simultaneously shifts its concentration both later in the preheat region and earlier in the reaction zone of the premixed flame, demonstrating the

complexity of the effect. This corresponds to a relative increase in consumption between these regions, increasing the local concentration of O and OH, as seen in Figure 4. This has the effect of ultimately increasing the local rate of fuel consumption, increasing the overall flame speed by a small amount.

This effect is not observed in the non-premixed flame—though updating the transport properties changes the structure of the oxidizer stream as it enters the flame zone, these structural changes are confined to a very small region near the oxidizer inlet. In this region, $O_2(a^1\Delta_g)$ rapidly quenches to $O_2(X^3\Sigma_g^-)$ though collisions before it can interact with any species that would come from the fuel, such as H, and most of the $O_2(a^1\Delta_g)$ is destroyed within 3 mm of the oxidizer inlet. Because of this, the production of radical species such as O is not altered significantly enough to have an effect on the flame. This demonstrates that the transport properties of excited singlet oxygen does not influence flames beyond its ability to interact with fuel, though it most significantly impacts its own transport, and this can have implications for kinetic experiments that attempt to track $O_2(a^1\Delta_g)$ as a function of space and time.

4.1 Appropriateness of the 6-12 Lennard-Jones model

An observation during the course of this investigation is that the molecular interactions of the excited state species did not strictly conform to the 6-12 Lennard-Jones potential. For the He-He* interaction in Figure 1, a local maximum beyond the short-range attraction was calculated, and this was also reported by Buckingham and Dalgarno [16]. A plot showing the unfitted interaction energies of $O_2(X^3\Sigma_g^-)$, $O_2(a^1\Delta_g)$, and $O_2(b^1\Sigma_g^+)$ is shown in Figure 8 for an "X" collision between the molecules.

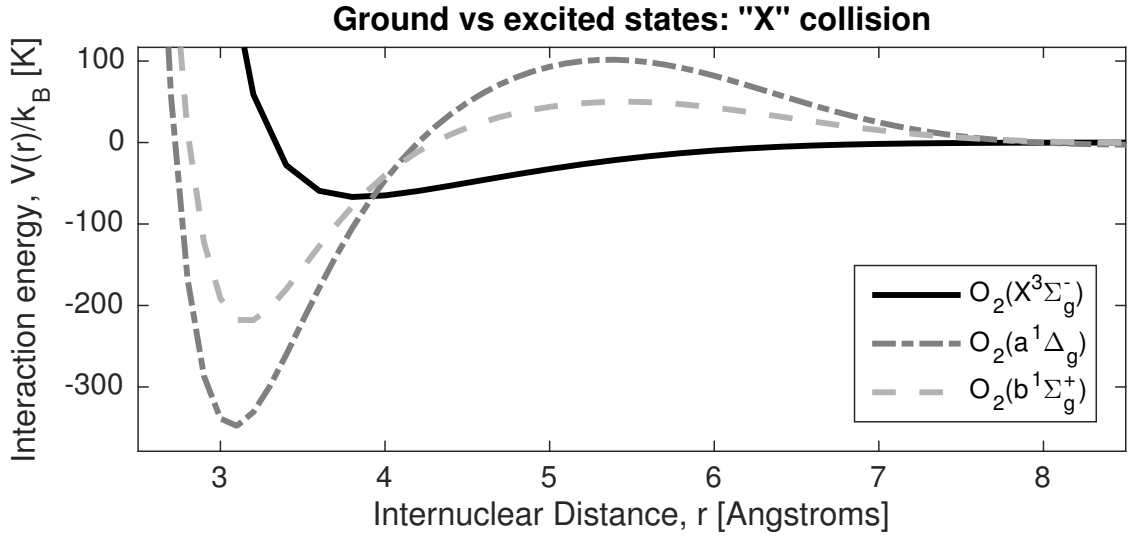

Figure 8: Comparison of the energies for $O_2(X^3\Sigma_g^-)$, $O_2(a^1\Delta_g)$, and $O_2(b^1\Sigma_g^+)$ as a function of intermolecular distance for an"X" collision.

A significant local maximum in the interaction energies for the two singlet states is observable at an intermolecular distance of approximately 5–6 Å, even larger than the original well depth ϵ/k_B

of ground state oxygen. As has been discussed and demonstrated in this paper, even significant differences in the transport properties of these excited state species does not strongly influence the outcome of steady laminar flame simulations; however, it is possible that this deviation from the 6-12-Lennard-Jones behavior has a more significant impact on kinetic investigations that utilize larger concentrations of excited oxygen in other applications. More thorough ab initio chemistry work is necessary to corroborate and confirm these findings before attempting to employ alternative transport models in future simulations.

5 Conclusion

Ab initio quantum chemistry methods to compute polarizabilities and molecular interactions between both ground state and excited state molecules are discussed, and the results are shown for calculations of the interactions of the ground states and the lowest lying excited states of O_2 and He. The inability of the methods to both qualitatively *and* quantitatively reproduce previous literature calculations of He-He* remains a concern and will be investigated in future work, but the results for ground state interactions show modest agreement with experimental values, granting us some confidence in the methods we used to determine the transport properties of excited state species. Additionally, we observed that excited state interactions do not strictly conform to the 6-12 Lennard-Jones model, or any model that is commonly used in combustion simulations. Though this is not expected to significantly impact flame simulations, it remains a finding of interest in regards to molecular dynamics.

After obtaining new transport properties from the intermolecular interactions, we then implemented the updated properties of $O_2(a^1\Delta_g)$ and $O_2(b^1\Sigma_g^+)$ in one dimensional flame simulations to demonstrate their effect on flame speed and structure. The effect of updating the transport properties is small, representing an approximately 0.25% change in overall flame speed and a 2% change in peak consumption rate of $O_2(a^1\Delta_g)$ in premixed flames. The updated transport properties do not appear to noticeably impact non-premixed flames beyond small regions in the oxidizer due to rapid collisional quenching.

The work presented demonstrates that varying the transport properties of excited state species in one dimensional steady flames has a small effect in the overall structure of the flames, suggesting that any current discrepancies between modeling and experiments is likely due to a so-far insufficient understanding of the chemical kinetics of these excited species. The small magnitude of the transport effect is likely due to the relatively small concentrations and short lifetimes of these species; however, it may have a noticeable effect at low pressures. These are conditions where kinetic studies are often performed, specifically because the lifetimes of the species of interest are longer and can be more readily observed experimentally. The effect of updating the transport properties is also likely to be more noticeable in conditions in which greater concentrations of $O_2(a^1\Delta_g)$ are present, such as is the case in ultra lean conditions of research interest, or in transient simulations of ignition by non-thermal plasma. The increased accuracy of the transport data can inform such chemical kinetic studies in the future.

Appendix

Collision orientations

Two molecules can collide with each other in an infinite number of orientations. Here, we only consider a head-on collision along a Cartesian axis aligned either parallel or perpendicular to the molecular bond of each O_2 molecule. For any two given identical linear molecules, if each is randomly oriented on one of the three Cartesian axes, there are 2 possible orientations on each of the 3 axes for each molecule, resulting in $6^2 = 36$ different combinations of orientations. However, O_2 is a homonuclear molecule, and so the number of distinguishable orientations for each molecule on an axis is half of the general case. If each O_2 molecule is randomly oriented on one of the three Cartesian axes, there are a total of $3^2 = 9$ different combinations of orientations to consider. But because O_2 is also symmetric about the axis of its double bond, the number of *unique* collisions is reduced significantly. In the restricted paradigm of orienting the molecules along Cartesian axes, there are four different collisions to consider, depicted in Figure 9. Since, of the 9 possible collisions, only 4 are unique, each of the unique orientations has a finite probability of occurring ($p \geq 1/9$), in the paradigm of an independently random (albeit restricted) orientation of each molecule. In a head on linear collision such as that depicted in Figure 9a, both molecules must be oriented on the collision axis. This collision has a probability of:

$$p_L = \frac{1}{3} \times \frac{1}{3} = \frac{1}{9} \tag{7}$$

A head on "T" collision such as that shown in Figure 9b can occur when one molecule is oriented along the collision axis and the other is oriented in either of the axes perpendicular to the collision axes. The probability is doubled because there are two molecules capable of occupying a given orientation,

$$p_T = \frac{1}{3} \times \frac{2}{3} + \frac{1}{3} \times \frac{2}{3} = \frac{4}{9} \tag{8}$$

This orientation of collision is the most likely to occur. The head on "sandwich" collision shown in Figure 9c occurs when both of the molecules are oriented along the same axis perpendicular to the collision axis. Because there are two axes perpendicular to the collision axis, this collision can occur in two ways.

$$p_S = \frac{1}{3} \times \frac{1}{3} + \frac{1}{3} \times \frac{1}{3} = \frac{2}{9} \tag{9}$$

The last type of collision, the "cross" collision shown in Figure 9d, can occur when both of the molecules are oriented on an axis perpendicular to the collision axis, but each molecule is aligned on a different axis. As with the "sandwich" collision, there are two different ways that this collision can occur.

$$p_X = \frac{1}{3} \times \frac{1}{3} + \frac{1}{3} \times \frac{1}{3} = \frac{2}{9} \tag{10}$$

In this restricted orientation paradigm, all of the types of collisions have thus been accounted for, since:

$$p_L + p_T + p_S + p_X = \frac{1}{9} + \frac{4}{9} + \frac{2}{9} + \frac{2}{9} = 1 \tag{11}$$

The results from the calculations of the intermolecular interaction energies for each type of collision are weighted accordingly, to produce an "average" potential that might be calculated from experimental observations.

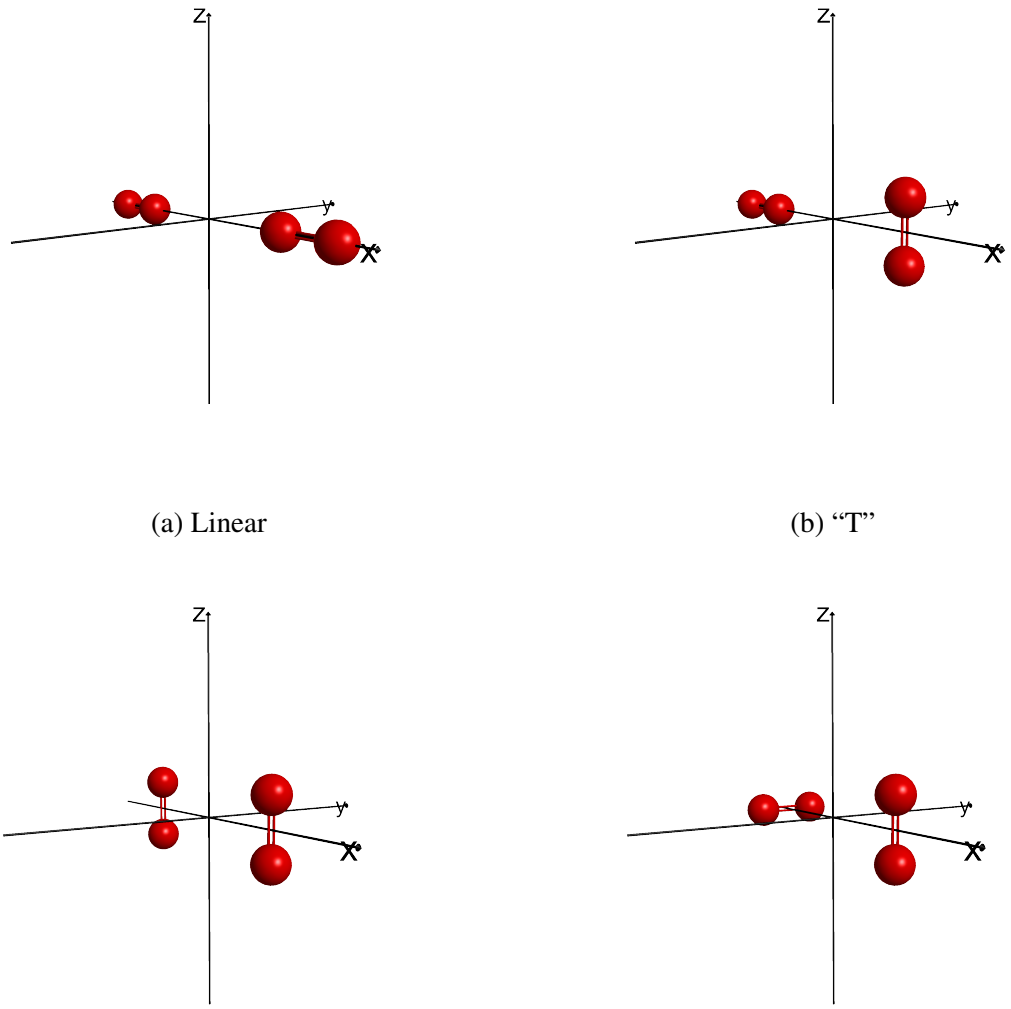

(a) Linear (b) "T"

(c) "Sandwich" (d) "X"

Figure 9: The four different orientations considered in these Potential Energy Surface scans; collision depicted here along the x-axis

Acknowledgments

This investigation conducted at University of California, Berkeley was supported in part by the National Science Foundation, Grant No. DGE 1106400, NSF/DOE Award No. CBET-1258653, and NSF Grant No. 1510709. Additionally, this research used resources of the National Energy Research Scientific Computing Center (NERSC), a DOE Office of Science User Facility supported by the Office of Science of the U.S. Department of Energy under Contract No. DE-AC02-05CH11231.

References

[1] J. Lawton and F.J. Weinberg. *Electrical Aspects of Combustion*. Oxford University Press, 1969.

[2] S M Starikovskaia. *J. Phys. D. Appl. Phys.*, 39 (2006) R265–R299.

[3] Andrey Starikovskiy and Nickolay Aleksandrov. *Prog. Energy Combust. Sci.*, 39 (2013) 61–110.

[4] Yiguang Ju and Wenting Sun. *Prog. Energy Combust. Sci.*, 48 (2015) 21–83.

[5] Benjamin Wolk, Anthony DeFilippo, Jyh-Yuan Chen, Robert Dibble, Atsushi Nishiyama, and Yuji Ikeda. *Combust. Flame*, 160 (2013) 1225–1234.

[6] Daniel I Pineda, Benjamin Wolk, Tim Sennott, Jyh-Yuan Chen, Robert W Dibble, and Daniel Singleton. Nanosecond Pulsed Discharge in a Lean Methane-Air Mixture. In *Laser Ignition Conf.*, Vol. C, page T5A.2, 2015.

[7] A. M. Starik, B. I. Loukhovitski, A. S. Sharipov, and N S Titova. *Philos. Trans. R. Soc. A Math. Phys. Eng. Sci.*, 373 (2015) 20140341.

[8] Alexander A. Konnov. *Combust. Flame*, 162 (2015) 3755–3772.

[9] A M Starik, V E Kozlov, and N S Titova. *J. Phys. D. Appl. Phys.*, 41 (2008) 125206.

[10] Timothy Ombrello, Sang Hee Won, Yiguang Ju, and Skip Williams. *Combust. Flame*, 157 (2010) 1916–1928.

[11] V E Kozlov, A M Starik, and N S Titova. *Combust. Explos. Shock Waves*, 44 (2008) 371–379.

[12] A. Bourig, D. Thévenin, J.-P. Martin, G. Janiga, and K. Zähringer. *Proc. Combust. Inst.*, 32 (2009) 3171–3179.

[13] A.M. Starik, V.E. Kozlov, and N.S. Titova. *Combust. Flame*, 157 (2010) 313–327.

[14] N A Popov. *Plasma Sources Sci. Technol.*, 20 (2011) 045002.

[15] Jie Han, Memdouh Belhi, and Fabrizio Bisetti. *Combust. Theory Model.*, 7830 (2015) 0–29.

[16] R. A. Buckingham and A. Dalgarno. *Proc. R. Soc. A Math. Phys. Eng. Sci.*, 213 (1952) 327–349.

[17] Donald Allan McQuarrie and John Douglas Simon. *Physical Chemistry: A Molecular Approach*. University Science Books, illustrate edition, 1997.

[18] Joseph O. Hirschfelder, Charles F. Curtiss, and R. Byron Bird. *Molecular Theory of Gases and Liquids*. John Wiley & Sons, Inc., New York, 2 edition, 1964.

[19] Jeffrey I. Steinfeld, Joseph S. Francisco, and William L. Hase. *Chemical Kinetics and Dynamics*. Prentice Hall, Upper Saddle River, NJ, 2nd edition, 1998.

[20] SI Sandler and JK Wheatley. *Chem. Phys. Lett.*, 10 (1971) 375–378.

[21] M.W. Schmidt, K Baldridge, J Boatz, S Elbert, M Gordon, J Jensen, S Koseki, N Matsunaga, K Nguyen, S Su, T Windus, M Dupuis, and J Montgomery. *J. Comput. Chem.*, 14 (1993) 1347–1363.

[22] Ahren W. Jasper and James a. Miller. *Combust. Flame*, 161 (2014) 101–110.

[23] Attila Szabo and Neil S. Ostlund. *Modern Quantum Chemistry: Introduction to Advanced Electronic Structure Theory*. McGraw-Hill, 1989.

[24] Thom H Dunning. *J. Chem. Phys.*, 90 (1989) 1007.

[25] C. C. J. Roothaan. *Rev. Mod. Phys.*, 32 (1960) 179–185.

[26] Bernard R. Brooks and Henry F. Schaefer. *J. Chem. Phys.*, 70 (1979) 5092.

[27] Jill E. Gready, G.B. Bacskay, and N.S. Hush. *Chem. Phys.*, 22 (1977) 141–150.

[28] Robert J. Kee, Fran M. Rupley, and J. A. Miller. CHEMKIN II: A FORTRAN Chemical Kinetics Package for the Analysis of Gas-phase Chemical Kinetics. Technical Report SAND-89-8009B, Sandia National Laboratories, Livermore, CA, USA, 1992.

[29] Robert J. Kee, James Miller, Mitchell D. Smooke, and Joseph F. Grcar. PREMIX: a Fortran program for modeling steady laminar one-dimensional premixed flames. Technical Report SAND85-8240, Sandia National Laboratories, Livermore, CA, USA, 1985.

[30] Andrew E Lutz, Robert J Kee, Joseph F Grcar, and Fran M Rupley. OPPDIF: A Fortran program for computing opposed-flow diffusion flames. Technical Report SAND96-8243, Sandia National Laboratories, Livermore, CA, USA, 1997.

[31] Anthony Cesar DeFilippo. *Microwave-Assisted Ignition for Improved Internal Combustion Engine Efficiency*. Phd dissertation, UC Berkeley, 2013.

[32] Gregory P. Smith, David M. Golden, Michael Frenklach, Nigel W. Moriarty, Boris Eiteneer, Mikhail Goldenberg, C. Thomas Bowman, Ronald K. Hanson, Soonho Song, William C. Gardiner, Vitali V. Lissianski, and Zhiwei Qin. GRI-MECH 3.0, 1999.

[33] Chung K. Law. *Combustion Physics*. Cambridge University Press, New York, 2006.

[34] Philip Rosen. *J. Chem. Phys.*, 18 (1950) 1182.